**Biophysical Journal, Volume *112***

## Supplemental Information

# Increased Tissue Stiffness in Tumors from Mice with Neurofibromatosis-1 Optic Glioma

**Christopher Walter, Lindsey Crawford, Melinda Lai, Joseph A. Toonen, Yuan Pan, Shelly Sakiyama-Elbert, David H. Gutmann, and Amit Pathak**

# Supporting Material

for

**"Increased Tissue Stiffness in Tumors From Mice with Neurofibromatosis-1 Optic Glioma"**

## Materials and Methods

### Mice and optic nerve dissection

Optic glioma-bearing (*Nf1*$^{flox/mut}$; GFAP-Cre) and WT (either *Nf1*$^{flox/flox}$ or C57BL/6) mice were bred and maintained at Washington University in accordance with an approved Animal Studies Protocol. For all experiments, 3-month-old mice were transcardially perfused with Ringer's solution, based on previous experiments demonstrating that gliomas are evident by this age (1). For AFM applications, optic nerves and chiasms were microdissected and placed in artificial cerebrospinal fluid (aCSF) until analyses were performed. For immunohistochemistry applications, mice were additionally perfused with 4% paraformaldehyde in 0.1 M sodium phosphate buffer (pH 7.4). Optic nerves and chiasms were microdissected and post-fixed in 4% paraformaldehyde. Samples were then embedded in paraffin and sectioned. For all glioma-bearing optic nerve experiments, optic nerves were observed under the microscope to confirm the presence of a glioma involving the chiasm.

### Atomic Force Microscopy

Dissected optic nerves were covalently attached to glass slides treated with Poly-L-Lysine (Sigma-Aldrich, St. Louis). Slides were pre-treated for at least 2 hours before attaching the optic

nerves. After attachment, optic nerves were kept in aCSF for the remainder of the experiment. All measurements were acquired using an MFP-3D-BIO atomic force microscope (Asylum Research, Santa Barbara, CA). In AFM, piezoelectric actuators are used to control the x, y, and z position of a probe, consisting of a flexible cantilever with a micron-sized tip attached to a chip. When the probe is near a surface, attractive and repulsive forces between the tip and the sample cause deflection of the cantilever, which is tracked by a laser reflected off the back of the cantilever onto a position-sensitive photodiode detector. To measure the elastic modulus of a sample, the sample (optic nerve surface) is indented by the probe, and the cantilever deflection is measured as a function of the probe's z position. Olympus TR400PB AFM probes with an Au/Cr coated silicon nitride cantilever and pyramidal tip (Asylum Research, Santa Barbara, CA), with reported stiffness of 0.02 N/m, were used to perform AFM on the optic nerves. Tips were initially calibrated in air to determine the spring constant of the cantilever. After determining the cantilever's spring constant, the probes were allowed to equilibrate in aCSF for at least 1 hour in order to prevent drift in the measured deflection due to the aCSF. Probes were then calibrated in aCSF in order to account for residual effects of the fluid during the testing process. To finish the setup procedure, the slides with the optic nerves in aCSF were then placed onto the AFM stage and probes were allowed to equilibrate in the aCSF for 15 min. AFM testing was performed by indenting nerves down the length and across the width of the optic nerves (**Fig. S1**).

To generate a force curve, the cantilever was first lowered close to the surface until a small deflection was measured due to surface interaction with the sample. When the system begins to generate a force curve, the probe approaches the tissue surface until a contact is made. After contact, the tip is indented into the sample until a user-defined threshold indentation force and depth are reached. The tip is then retracted from the sample and returned to its original position. In our measurements, typical force curves were generated by indenting nerves with a force of 10 nN through 2 μm of working distance. Indentation speed was set at 7 μm/s in

order to negate viscous effects of the aCSF. Force curves resembled those of typical viscoelastic materials, with a small contact region following the approach, followed by a linear indentation (**Fig. S1**). The retraction portion of the curve shows sticking behavior, as seen by separation from the indentation curve during the initial portion just past the contact point, where a quick jump is observed, representing the tip "unsticking" from the sample and returning to its original position. Any curves that did not exhibit this behavior were not analyzed.

A modified Hertz model, implemented in MATLAB, was used to analyze the force curves. The Hertz model assumes that the tip does not deform and the tissue sample is linear elastic and of infinite length (2, 3). The modified Hertz model is developed to analyze viscoelastic materials by first normalizing the approach portion of the indentation curve to 0 (4, 5). Then, the model determines the contact point, generates a best-fit curve for maximal overlap with the measured indentation curve, and computes the elastic modulus. This was repeated for 5 samples per condition (wild-type versus glioma-bearing nerves) and the 5 values were averaged.

**Immunohistochemistry**

Immunohistochemistry was performed on paraffin-embedded optic nerves and chiasms using anti-MMP-9 (1:500 dilution, Abcam ab38898), anti-MMP-2 (1:2000 dilution, Abcam ab110186), and anti-LOX (1:500 dilution, Abcam ab31238) primary antibodies. Antigen retrieval was accomplished in a citrate buffer (pH 6.0) at 100$^{o}$C for 15 minutes. Primary antibody detection was performed with biotinylated secondary antibodies (1:200 dilution, Vector labs), followed by amplification using peroxidase-conjugated avidin (Vectastain Elite ABC kit, Vector labs) and treatment with 3,3'-diaminobenzadine substrate kit (Vector labs). All samples were counterstained with hematoxylin. Sections were imaged at the chiasm and proximal optic nerve, and photographed at 20x using a Nikon Eclipse E600 inverted microscope equipped with a Leica EC3 camera. All studies were performed in triplicate. Quantification was performed by

counting positive and negative cytosolic staining using the cell counting application in NIH ImageJ software. Cells were scored as immunopositive when antibody-mediated cytosolic staining was observed, while the total number of cells were identified by hematoxylin counterstaining. For each antibody, 3 randomly-selected images representing 3 individual mice per genotype (9 images total) were counted.

**Quantitative real-time reverse transcribed RNA polymerase chain reaction (qRT-PCR).**

qRT-PCR was performed using mouse *Mmp2*-specific primers (forward: 5'-CAGGGAATGAGTACTGGGTCTATT; reverse: 5'-ACTCCAGTTAAAGGCAGCATCTAC) on *Nf1*-deficient and wild-type (WT) astrocytes (n=3 independent samples each) generated and analyzed as previously described (6, 7).

**Statistics**

Statistics for AFM were performed using a custom MATLAB script, utilizing a two-way ANOVA test. Groups were considered to show a statistically significant difference for p-values $< 0.05$. Statistics for immunohistochemistry were performed using a student's t-test

# Supplementary Figures

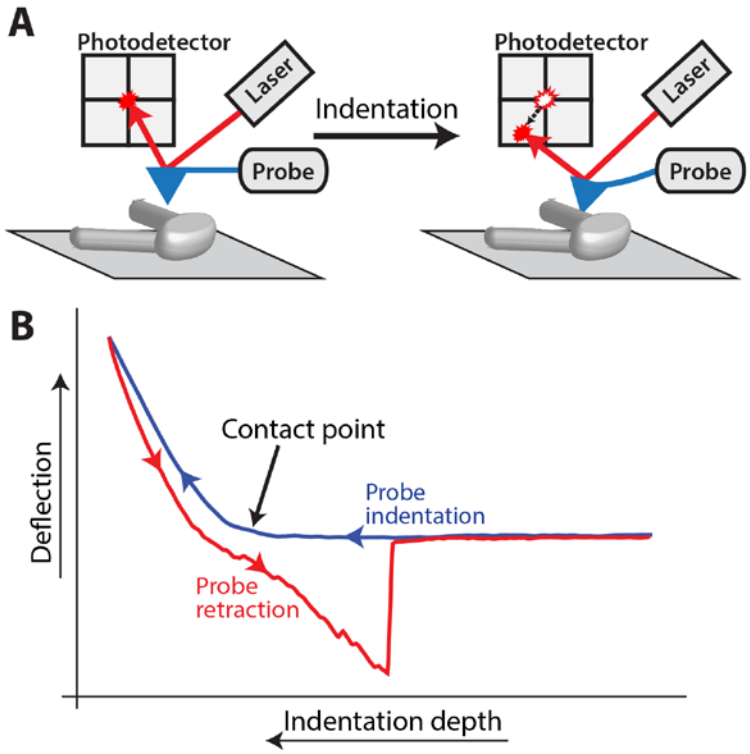


**Figure S1**. **Schematic depiction of AFM measurements in wild-type and *Nf1* glioma-bearing optic nerves**. **(A)** Graphic illustration of the methods used to obtain indentation curves by AFM. As the tip is lowered into the optic nerve sample, the spot where the laser strikes the photodetector changes, which is measured as a deflection. **(B)** Representative curves for probe indentation (blue) and retraction (red) on an optic nerve surface. Black arrow indicates the contact point for the probe.

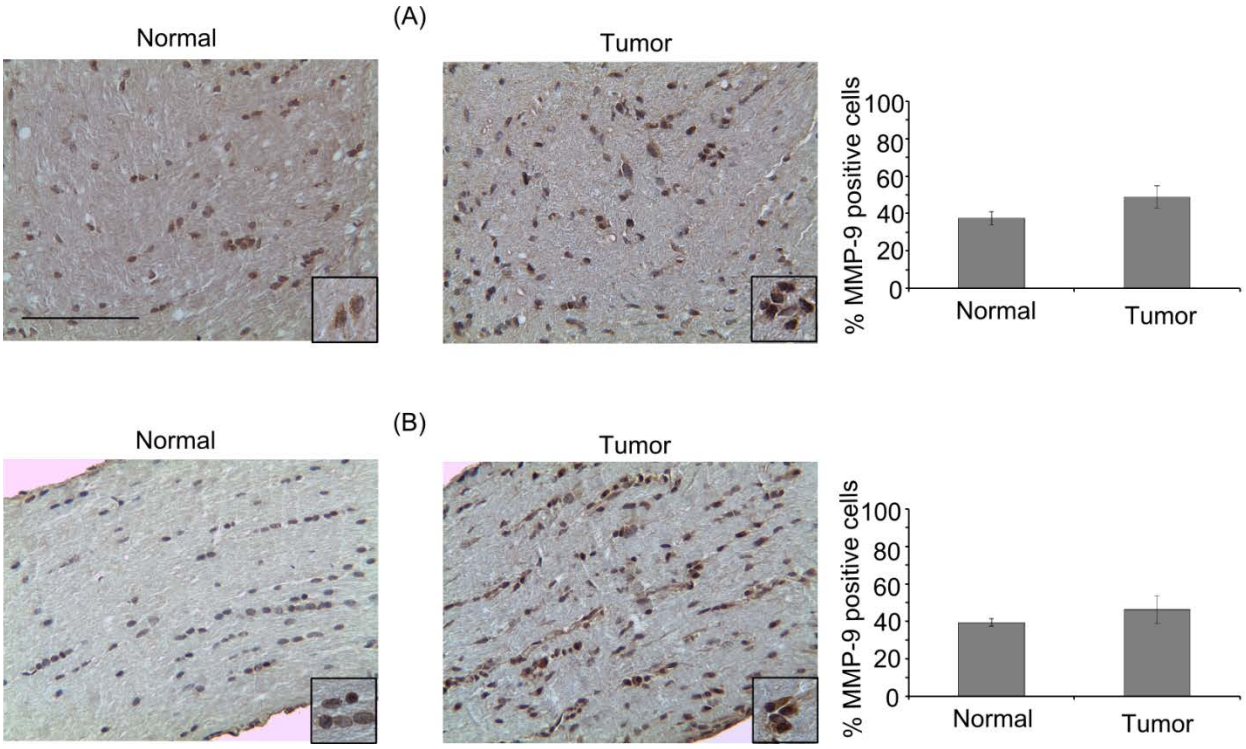


**Figure S2.** Glioma-bearing optic nerves show no change in MMP-9 expression relative to healthy optic nerves (normal) in both the chiasm (A) and optic nerve (B). Error bars represent SEM. Scale bar, 100 µm.

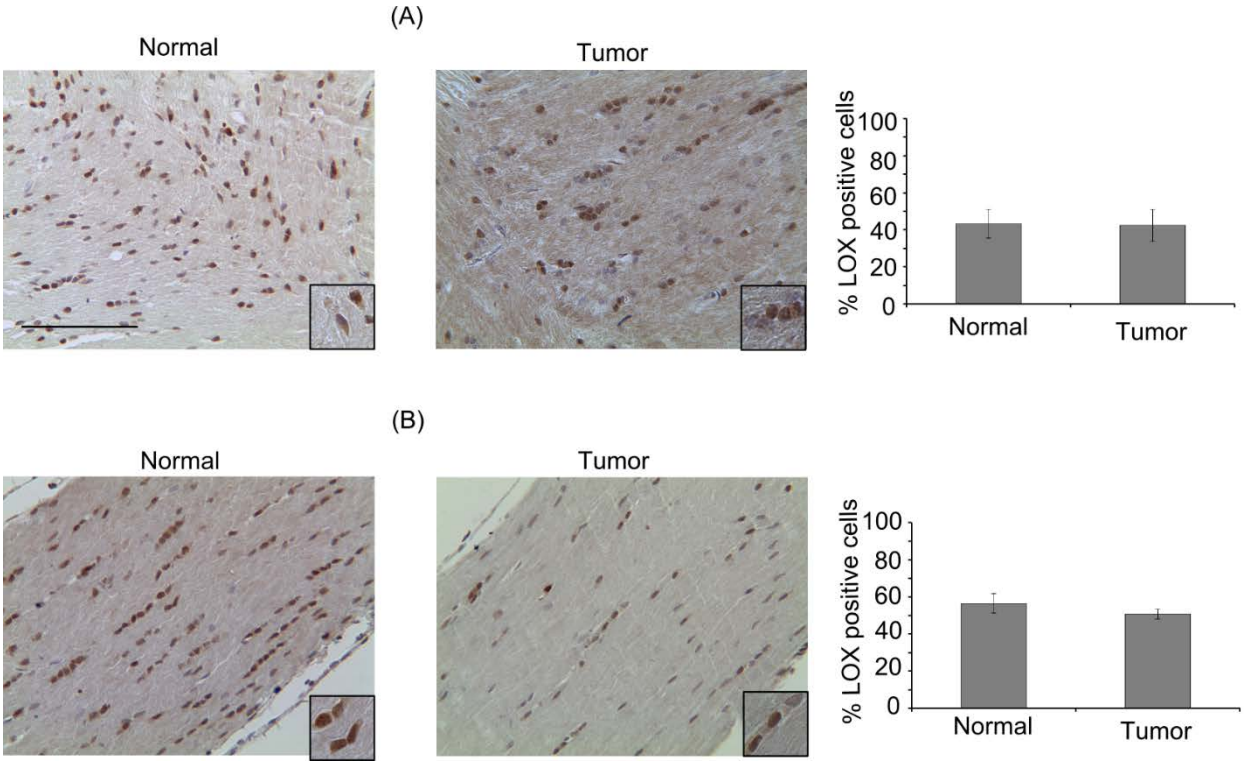


**Figure S3.** Glioma-bearing optic nerves show no change in LOX expression relative to healthy optic nerves (normal) in both the chiasm (A) and the optic nerve (B). Error bar represent SEM. Scale bar, 100 µm.

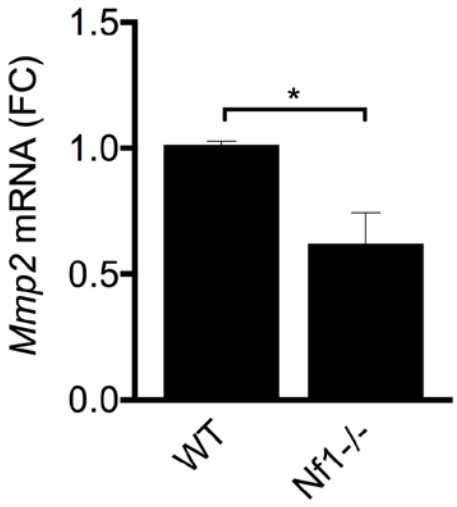


**Figure S4.** qRT-PCR analysis reveals a 40% decrease in *Mmp2* expression in *Nf1*-deficient astrocytes relative to their wild-type (WT) counterparts (n=3 samples each; p=0.033).

# References


1. Toonen, J. A., Y. Ma, and D. H. Gutmann. 2016. Defining the temporal course of murine neurofibromatosis-1 optic gliomagenesis reveals a therapeutic window to attenuate retinal dysfunction. Neuro Oncol.
2. Bilodeau, G. G. 1992. Regular Pyramid Punch Problem. Journal of Applied Mechanics 59:519-523.
3. Li, Q. S., G. Y. H. Lee, C. N. Ong, and C. T. Lim. 2008. AFM indentation study of breast cancer cells. Biochemical and Biophysical Research Communications 374:609-613.
4. Mackay, J. L., and S. Kumar. 2013. Measuring the elastic properties of living cells with atomic force microscopy indentation. Methods Mol Biol 931:313-329.
5. Dimitriadis, E. K., F. Horkay, J. Maresca, B. Kachar, and R. S. Chadwick. 2002. Determination of elastic moduli of thin layers of soft material using the atomic force microscope. Biophysical journal 82:2798-2810.
6. Solga, A. C., W. W. Pong, K. Y. Kim, P. J. Cimino, J. A. Toonen, J. Walker, T. Wylie, V. Magrini, M. Griffith, O. L. Griffith, A. Ly, M. H. Ellisman, E. R. Mardis, and D. H. Gutmann. 2015. RNA Sequencing of Tumor-Associated Microglia Reveals Ccl5 as a Stromal Chemokine Critical for Neurofibromatosis-1 Glioma Growth. Neoplasia 17:776-788.
7. Smithson, L. J., and D. H. Gutmann. 2016. Proteomic analysis reveals GIT1 as a novel mTOR complex component critical for mediating astrocyte survival. Genes & Development 30:1383-1388.